

Electric displacement as the fundamental variable in electronic-structure calculations

Massimiliano Stengel,¹ Nicola A. Spaldin,¹ and David Vanderbilt²

¹*Materials Department, University of California, Santa Barbara, CA 93106-5050, USA*

²*Department of Physics and Astronomy, Rutgers University, Piscataway, New Jersey 08854-8019, USA*
(Dated: June 4, 2008)

Finite-field calculations in periodic insulators are technically and conceptually challenging, due to fundamental problems in defining polarization in extended solids. While significant progress has been made recently with the establishment of techniques to fix the electric field \mathcal{E} or the macroscopic polarization \mathbf{P} in first-principles calculations, both methods lack the ease of use and conceptual clarity of standard zero-field calculations. Here we develop a new formalism in which the electric displacement \mathbf{D} , rather than \mathcal{E} or \mathbf{P} , is the fundamental electrical variable. Fixing \mathbf{D} has the intuitive interpretation of imposing open-circuit electrical boundary conditions, which is particularly useful in studying ferroelectric systems. Furthermore, the analogy to open-circuit capacitors suggests an appealing reformulation in terms of free charges and potentials, which dramatically simplifies the treatment of stresses and strains. Using PbTiO_3 as an example, we show that our technique allows full control over the electrical variables within the density functional formalism.

The development of the modern theory of polarization [1] has fueled exciting progress in the theory of the ferroelectric state. Many properties that could previously be inferred only at a very qualitative level can now be computed with quantum-mechanical accuracy within first-principles density-functional theory. Early *ab-initio* studies focused on bulk ferroelectric crystals, elucidating the delicate balance between covalency and electrostatics that gives rise to ferroelectricity. Over time, these methods were extended to treat the effects of external parameters such as strains or electric fields [2, 3]. Of particular note is the recent introduction by Diéguez and Vanderbilt [4] of a method for performing calculations at fixed macroscopic polarization \mathbf{P} . The ability to compute crystal properties from first principles as a function of \mathbf{P} provides an intuitive and appealing link to Landau-Devonshire and related semiempirical theories in which \mathbf{P} serves as an order parameter.

Despite its obvious appeal, however, the constrained- \mathbf{P} method has found limited practical application to date. One reason for this is that the procedure to enforce a constant \mathbf{P} during the electronic self-consistency cycle is relatively involved; this hampers the study of complex heterostructures with large supercells, where computational efficiency is crucial. There are also physical reasons. In particular, fixing \mathbf{P} does not correspond to experimentally realizable electrical boundary conditions (Fig. 1). Moreover, in an inhomogeneous heterostructure, the local polarization can vary from one layer to another, and its average is therefore best regarded as a derived, not a fundamental, quantity. In the following we show that considering \mathbf{D} as the fundamental electrical variable overcomes these physical limitations, and that constraining \mathbf{D} rather than \mathbf{P} leads to a simpler implementation.

Formalism. We consider a periodic insulating crystal defined by three primitive translation vectors \mathbf{a}_i , with Ω

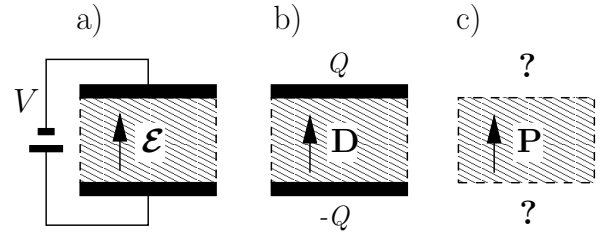


FIG. 1: Electrical boundary conditions within different methods. a) The fixed- \mathcal{E} method corresponds to adopting closed-circuit boundary conditions with a constant applied bias V . b) Constraining \mathbf{D} corresponds to a capacitor in open-circuit conditions with a fixed value of the free charge Q on the plates. c) constraining \mathbf{P} does not correspond to a clear experimental set-up.

the unit cell volume, and we introduce the new functional

$$U(\mathbf{D}, v) = E_{\text{KS}}(v) + \frac{\Omega}{8\pi} [\mathbf{D} - 4\pi\mathbf{P}(v)]^2. \quad (1)$$

$U(\mathbf{D}, v)$ depends directly on an external vector parameter \mathbf{D} , and indirectly on the internal (ionic and electronic) coordinates v through the Kohn-Sham energy E_{KS} and the Berry-phase polarization \mathbf{P} [1]. (For the moment we fix the lattice vectors; strains will be discussed shortly.) The minimum of U at fixed \mathbf{D} is given by the stationary point where all the gradients with respect to v vanish,

$$\left. \frac{\partial U}{\partial v} \right|_{\mathbf{D}} = \frac{\partial E_{\text{KS}}}{\partial v} - \Omega (\mathbf{D} - 4\pi\mathbf{P}) \cdot \frac{\partial \mathbf{P}}{\partial v} = 0. \quad (2)$$

Comparing with the fixed- \mathcal{E} approach of Ref. [2, 3] in which the electric enthalpy \mathcal{F} is given by

$$\mathcal{F}(\mathcal{E}, v) = E_{\text{KS}}(v) - \Omega \mathcal{E} \cdot \mathbf{P}(v), \quad (3)$$

we see that

$$\left. \frac{\partial \mathcal{F}}{\partial v} \right|_{\mathcal{E}} = \left. \frac{\partial U}{\partial v} \right|_{\mathbf{D}} \quad (4)$$

provided that we set $\boldsymbol{\mathcal{E}} = \mathbf{D} - 4\pi\mathbf{P}$. We thus discover that $\mathbf{D} = \boldsymbol{\mathcal{E}} + 4\pi\mathbf{P}$ is the macroscopic electric displacement field. The functional in Eq. (1) takes the form $U = E_{\text{KS}} + (\Omega/4\pi)\boldsymbol{\mathcal{E}}^2$, which is the correct expression for the internal energy of a periodic crystal when a uniform external field is present (details are given in Supplementary Section 2.4). Eq. (1) thus provides a framework for finding the minimum of the internal energy $U(\mathbf{D})$ with respect to all internal degrees of freedom at specified electric displacement \mathbf{D} . This is the essence of our constrained- \mathbf{D} method.

As a consequence of Eq. (4), the method is analogous to a standard finite- $\boldsymbol{\mathcal{E}}$ -field calculation [2, 3]. In particular, the Hellmann-Feynman forces are computed in the same way. The only difference is that the value of $\boldsymbol{\mathcal{E}}$, instead of being kept constant, is updated at every iteration until the target value of \mathbf{D} is obtained at the end of the self-consistency cycle (or ionic relaxation). This implies that the implementation and use of the constrained- \mathbf{D} method in an existing finite- $\boldsymbol{\mathcal{E}}$ -field code is immediate; in our case it required the modification of *two lines* of code only.

The effect of constraining \mathbf{D} , rather than $\boldsymbol{\mathcal{E}}$, essentially corresponds to the imposition of longitudinal, rather than transverse, electrical boundary conditions. For example, as we shall see below, the phonon frequencies obtained from the force-constant matrix computed at fixed \mathbf{D} are the longitudinal optical (LO) ones, while the usual approach yields instead the transverse optical (TO) frequencies. Furthermore, the longitudinal electrical boundary conditions are appropriate to the physical realization of an *open-circuit* capacitor with fixed free charge on the plates, while the usual approach applies to a closed-circuit one with a fixed voltage across the plates (Fig. 1).

Stress tensor. This analogy with an open-circuit capacitor suggests an intuitive strategy for deriving the stress tensor, a quantity that plays a central role in piezoelectric materials. In particular, the electrode of an isolated open-circuit capacitor cannot exchange *free* charge with the environment. This suggests that the *flux* of the vector field \mathbf{D} through the three independent facets of the primitive unit cell should remain constant under an applied strain. These fluxes are $\mathbf{a}_i \times \mathbf{a}_j \cdot \mathbf{D} = \Omega \mathbf{b}_i \cdot \mathbf{D}$, where the \mathbf{b}_i are duals ($\mathbf{a}_i \cdot \mathbf{b}_j = \delta_{ij}$) differing by a factor of 2π from the conventional reciprocal lattice vectors. We then rewrite the functionals in terms of the “internal” or “reduced” variables $d_i = (\Omega/4\pi)\mathbf{b}_i \cdot \mathbf{D}$. It is also useful to define the reduced polarization $p_i = \Omega \mathbf{b}_i \cdot \mathbf{P}$ and the “dual” reduced electric field $\bar{\varepsilon}_i = \mathbf{a}_i \cdot \boldsymbol{\mathcal{E}}$. Additional details are provided in the Supplementary Section 4.

By Gauss’s law, $d_i = -Q_i$, where the Q_i are the free charges per surface unit cell located on the cell face normal to \mathbf{b}_i . With these definitions, the internal energy can be rewritten as

$$U(\{d_i\}) = E_{\text{KS}} + \frac{2\pi}{\Omega} \sum_{ij} (d_i - p_i) g_{ij} (d_j - p_j) \quad (5)$$

where we have introduced the metric tensor $g_{ij} = \mathbf{a}_i \cdot \mathbf{a}_j$. We then define the fixed- $\{d_i\}$ stress tensor as

$$\sigma_{\mu\nu} = \frac{1}{\Omega} \left(\frac{dU}{d\eta_{\mu\nu}} \right)_{\{d_i\}} \quad (6)$$

where $\eta_{\mu\nu}$ is the strain tensor. By a Hellmann-Feynman argument (see Supplementary Section 4.3) the total derivative in Eq. (6) can be replaced by a partial derivative. Using $dg_{ij}/d\eta_{\mu\nu} = 2a_{iu}a_{jv}$, we find

$$\sigma_{\mu\nu} = \sigma_{\mu\nu}^{\text{KS}} + \sigma_{\mu\nu}^{\text{Max}} + \sigma_{\mu\nu}^{\text{aug}}, \quad (7)$$

where $\sigma_{\mu\nu}^{\text{KS}}$ is the standard zero-field expression,

$$\sigma_{\mu\nu}^{\text{Max}} = \frac{2\mathcal{E}_\mu\mathcal{E}_\nu - \delta_{\mu\nu}\mathcal{E}^2}{8\pi} \quad (8)$$

is the Maxwell stress tensor (which originates from the derivative acting on g_{ij} and Ω^{-1}), and

$$\sigma_{\mu\nu}^{\text{aug}} = - \left(\frac{4\pi}{\Omega} \right)^2 \sum_i \bar{\varepsilon}_i \frac{\partial p_i}{\partial \eta_{\mu\nu}} \quad (9)$$

is the “augmented” part. If the internal variables v are chosen as reduced atomic coordinates and plane-wave coefficients in a norm-conserving pseudopotential context, neither the ionic nor the Berry-phase component of p_i has any explicit dependence on strain, and $\sigma_{\mu\nu}^{\text{aug}}$ vanishes. The name thus refers to the fact that $\sigma_{\mu\nu}^{\text{aug}}$ is nonzero only in ultrasoft pseudopotential [5] and projector augmented-wave [6] contexts. We note that, as a consequence of fixing the reduced variables d_i rather than the Cartesian \mathbf{D} , the *proper* treatment of piezoelectric effects [7, 8] is automatically enforced.

Legendre transformation. The transformation from variables \mathbf{D} to variables $\boldsymbol{\mathcal{E}}$ can be regarded as part of a Legendre transformation. We spell out this connection here, working instead with reduced variables (d_1, d_2, d_3) and $(\bar{\varepsilon}_1, \bar{\varepsilon}_2, \bar{\varepsilon}_3)$. First, we note that

$$\frac{dU}{dd_i} = \frac{\partial U}{\partial d_i} = \bar{\varepsilon}_i. \quad (10)$$

Recall that $\bar{\varepsilon}_i = \mathbf{a}_i \cdot \boldsymbol{\mathcal{E}}$, so that $-\bar{\varepsilon}_i$ is just the potential step V_i encountered while moving along lattice vector \mathbf{a}_i , while Q_i is just the free charge on cell face i . Thus, when the system undergoes a small change at fixed $(\bar{\varepsilon}_1, \bar{\varepsilon}_2, \bar{\varepsilon}_3)$, the work done by the battery is $-\sum_i V_i dQ_i = -\sum_i \bar{\varepsilon}_i dd_i$. We therefore define

$$\tilde{\mathcal{F}}(\bar{\varepsilon}_1, \bar{\varepsilon}_2, \bar{\varepsilon}_3) = \min_{d_1, d_2, d_3} [U(d_1, d_2, d_3) - \sum_i \bar{\varepsilon}_i d_i], \quad (11)$$

where the potentials $\bar{\varepsilon}_i$ have become the new independent variables and d_i are now implicit in the minimum condition. The energy functionals $U(\{d_i\})$ and $\tilde{\mathcal{F}}(\{\bar{\varepsilon}_i\})$ thus form a Legendre-transformation pair.

All the gradients with respect to the internal and strain degrees of freedom are preserved by the Legendre transformation and need not be rederived for $\tilde{\mathcal{F}}$. The physical electrical boundary conditions, however, have changed back to the *closed-circuit* case. It is therefore natural to expect the functional $\tilde{\mathcal{F}}$ to be closely related to the fixed- \mathcal{E} enthalpy \mathcal{F} of Eq. (3). Indeed, it is straightforward to show that

$$\tilde{\mathcal{F}} = U - \frac{\Omega}{4\pi} \mathcal{E} \cdot \mathbf{D} = \mathcal{F} - \frac{\Omega}{8\pi} \mathcal{E}^2. \quad (12)$$

At fixed strain and $\bar{\varepsilon}_i$, the $\Omega \mathcal{E}^2/8\pi$ term is constant, and thus does not contribute to the gradients with respect to the internal variables, consistent with Eq. (4). However, the stress derived from \mathcal{F} differs from the one derived from $\tilde{\mathcal{F}}$ by the Maxwell term $\sigma_{\mu\nu}^{\text{Max}}$, which is absent in \mathcal{F} (details of the derivation are provided in Supplementary Section 4.3). Although the Maxwell stress is tiny on the scale of typical first-principles calculations (e.g. 10^8 V/m produces a pressure of 44.3 KPa), for reasons of formal consistency we encourage the use of $\tilde{\mathcal{F}}$ in place of \mathcal{F} in future works.

Partial Legendre transformations. It is also possible to define hybrid thermodynamic functionals via partial Legendre transformations that act only on one or two of the three electrical degrees of freedom. Of most interest is the case of two fixed V and one fixed Q , i.e., functions of variables $(\bar{\varepsilon}_1, \bar{\varepsilon}_2, d_3)$. The special direction is denoted by unit vector $\hat{\mathbf{q}}$ which is along direction \mathbf{b}_3 . When $\bar{\varepsilon}_1 = \bar{\varepsilon}_2 = 0$, this applies to two common experimental situations: the case of an insulating film sandwiched in the $\hat{\mathbf{q}}$ direction between parallel electrodes in open-circuit boundary conditions, and the case of a long-wavelength LO phonon of wavevector \mathbf{q} where the $\mathbf{q} \rightarrow 0$ limit is taken along direction $\hat{\mathbf{q}}$.

This latter case of LO phonons exemplifies the physical interpretation of our method and its usefulness. While the *gradients* of U and its partially Legendre-transformed partner are identical, the *force constant matrices*, which are second derivatives, are not. Indeed, the force-constant matrices are found to differ by

$$\Delta K_{I\alpha, J\beta} = \frac{4\pi}{\Omega} \frac{(\mathbf{Z}_I \cdot \hat{\mathbf{q}})_\alpha (\mathbf{Z}_J \cdot \hat{\mathbf{q}})_\beta}{\hat{\mathbf{q}} \cdot \epsilon_\infty \cdot \hat{\mathbf{q}}}, \quad (13)$$

where $I\alpha$ labels the atom I and its displacement direction α , $\mathbf{Z}_{I\alpha}$ is the corresponding dynamical charge, and ϵ_∞ is the purely electronic dielectric tensor. This is readily identified as the non-analytic contribution to the LO-TO splitting of a phonon of small wavevector \mathbf{q} in the theory of lattice dynamics [9]. Thus, it becomes straightforward to obtain zone-center LO frequencies by direct finite-difference calculations at fixed \mathbf{D} , as will be demonstrated shortly.

Dielectric tensor and linear response. This scheme lends itself naturally to the perturbative linear-response analysis of the second derivatives of the internal energy

as described in Ref. [8], with two important differences. First, in our scheme the derivatives at constant \mathbf{D} become the elementary tensors, while the derivatives at constant \mathcal{E} are “second-level” quantities; this is an advantage, since using \mathbf{D} as independent variable is very convenient in ferroelectric systems. Second, the use of the reduced field variables d_i and $\bar{\varepsilon}_i$ in place of the macroscopic vector fields \mathbf{P} and \mathcal{E} makes the discussion of strains under an applied field much more rigorous and intuitive.

As an example of the relationship between constrained- $\bar{\varepsilon}$ and constrained- d tensors it is useful to introduce the inverse capacitance, $\gamma = C^{-1}$, in matrix form as

$$\gamma_{ij} = \frac{d^2 U}{dd_i dd_j}. \quad (14)$$

Incidentally, while this expression is fully general and well-defined in the non-linear regime, for the special case of a linear medium we can write

$$U = U_0 + \frac{1}{2} \sum_{ij} \gamma_{ij} Q_i Q_j, \quad (15)$$

which generalizes the textbook formula $U = Q^2/2C$ to the case of three mutually coupled capacitors. It can be shown that the same information can be obtained within the constrained- $\bar{\varepsilon}$ approach by means of the relationship

$$(\gamma^{-1})_{ij} = \frac{d^2 \tilde{\mathcal{F}}}{d\bar{\varepsilon}_i d\bar{\varepsilon}_j}. \quad (16)$$

The matrix γ_{ij} can be thought of a “reduced” representation of the macroscopic dielectric tensor,

$$(\epsilon^{-1})_{\alpha\beta} = \frac{\Omega}{4\pi} \sum_{i,j} \gamma_{ij} b_{i,\alpha} b_{j,\beta}, \quad (17)$$

or equivalently

$$\epsilon_{\alpha\beta} = \frac{4\pi}{\Omega} \sum_{i,j} (\gamma^{-1})_{ij} a_{i,\alpha} a_{j,\beta}. \quad (18)$$

We will consider, in addition to the *total* static capacitance above, the closely related frozen-strain γ_{ij}^η and frozen-ion γ_{ij}^∞ tensors. The remainder of the response functions discussed in Ref. [8] can be similarly defined in terms of the second derivatives of $U(\{d\}, u, \eta)$.

Applications. In the following we illustrate our method by computing the electrical equation of state of a prototypical ferroelectric material, PbTiO_3 . Our calculations are performed within the local-density approximation [10] (LDA) of density-functional theory using norm-conserving [11] pseudopotentials and a planewave cutoff of 150 Ry. The tetragonal unit cell contains one formula unit, and a $6 \times 6 \times 6$ Monkhorst and Pack [12] grid is used to sample the Brillouin zone. The finite electric field is applied through a Wannier-based real-space technique [13], which converges quickly as a function of k -point mesh resolution [14]; indeed, tests made with finer

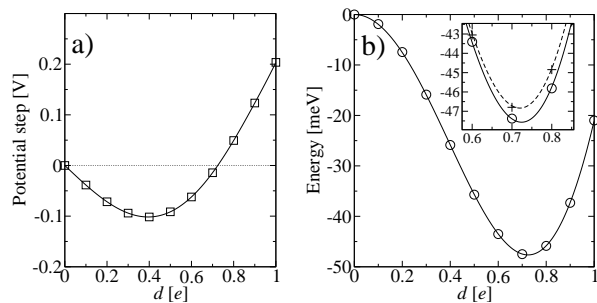


FIG. 2: Potential step and internal energy as a function of d . Symbols, calculated using constrained- \mathbf{D} method: (a) reduced electric field $\bar{\varepsilon}$ (squares); (b) internal energy U (circles). Solid curves: (a) numerical cubic spline fit to the symbols; (b) numerical integral of the spline fit in (a). Inset: enlargement near the minimum, also showing magnitude of the error made if Pulay stresses are neglected (dashed curve).

meshes showed no differences within numerical accuracy. We obtain an equilibrium lattice constant of $a=3.879$ Å for cubic paraelectric PbTiO_3 , in line with values previously reported in the literature. Due to the tetragonal symmetry, the state of the system is fully determined by six parameters: the electric displacement d , the cell parameters a and c , and three internal coordinates describing relative displacements along z .

Starting from the relaxed cubic structure in zero field, we calculate the equilibrium state for ten evenly spaced values of the reduced displacement d , ranging from $d=0.1e$ to $d=1.0e$ (where $-e$ is the electron charge), and relaxing all the structural variables at each d value. We set a stringent accuracy threshold of 10^{-5} Ha/bohr for atomic forces and 10^{-7} Ha/bohr³ for stresses. First we check the internal consistency of the formalism by verifying that our calculated potential drop $\bar{\varepsilon}$ coincides with the numerical derivative of U with respect to d as expected from Eq. (10). The comparison is shown in Fig. 2, where the discrepancies, of order 10^{-6} Ha, are not even visible. This confirms the internal consistency of the formalism and the high numerical accuracy of the calculations. The minimum in Fig. 2 (b) [which coincides with the zero-crossing in (a)] at $d = 0.725e$ corresponds to a spontaneous polarization of $P_s = 0.78$ C/m².

We note that this comparison is sensitive to the Pulay stress, even in the present case where our conservative choice of the plane-wave cutoff makes this error as small as $\pi_P = 82$ MPa. Neglecting such error corresponds to applying a hydrostatic pressure of $-\pi_P$, which leads to a discrepancy between the integrated potential (dashed curve in the inset of Fig. 2) and the calculated internal energy values. The agreement can be restored by plotting, instead of U (circles), the correct functional $U + \pi_P \Omega$ for constant-pressure conditions (plus symbols). (Of course, an analogous procedure can be used to simulate an arbitrary external pressure applied to the system.) As such,

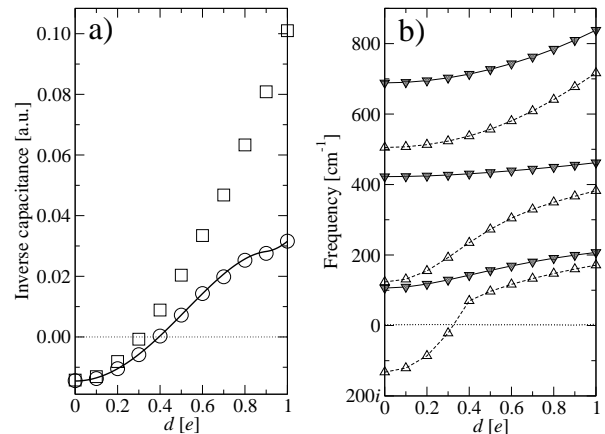


FIG. 3: Dielectric and lattice-dynamical properties. (a) Calculated inverse capacitance in the free-stress γ (circles) and fixed strain γ^n (squares) limits. The points were obtained by extracting the symmetric 6×6 elementary response tensors by finite differences (steps of ± 0.001 were taken for each parameter) for each value of d ; the continuous curve is the result of numerical differentiation of the splined potential. (b) Longitudinal (filled symbols, continuous curves) and transverse (open symbols, dashed curves) optical modes of Γ_{15} symmetry as a function of d .

this comparison constitutes a stringent test that all numerical issues have been properly accounted for, particularly in systems like PbTiO_3 that are characterized by a strong piezoelectric response.

Having verified the accuracy and consistency of our method, we now demonstrate its utility by analyzing the second derivative of the internal energy (or equivalently the first derivative of the potential) as a function of d , which corresponds to the inverse capacitance γ . The symbols in Fig. 3(a) show the linear-response values of both γ^n and γ , which are identical in the non-piezoelectric cubic limit. The numerical derivative of the splined potential of Fig. 2(a) accurately matches γ , again confirming the high numerical quality of our calculations. Fig. 3(a) shows that the inverse capacitance is *negative* for $0 < d < 0.395$ [the zero-crossing point corresponds to the inflection point of the $U(d)$ curve of Fig. 2(b), and to the minimum of $\bar{\varepsilon}(d)$ of Fig. 2(a)]. This is indicative of the fact that cubic PbTiO_3 is characterized by a ferroelectric instability, which means that the $U(d)$ curve has a negative curvature around the saddle point $d = 0$. We suggest, therefore, that the constrained- \mathbf{D} inverse capacitance at $d = 0$, while not accessible experimentally (since it corresponds to an unstable configuration of the crystal), is a useful indicator of the *strength* of the ferroelectric instability. As such, it can play an important role in determining the *critical thickness* for ferroelectricity in thin perovskite films; in particular, a material with lower γ should be ferroelectric down to smaller thicknesses. Note that in our terminology one ferroelectric

can be both *stronger* and *less polar* than another if it has a more negative γ but a smaller $|P_s|$.

Finally, to further elucidate the capabilities of our method, for each value of d we diagonalize both the longitudinal (directly obtained by finite differences) and transverse (obtained by using the additional ΔK term as defined in Eq. 13) dynamical matrices, and plot in Fig. 3 (b) the resulting normal mode frequencies. This analysis shows very clearly the crossover point when the frequency of the “soft” TO1 mode becomes imaginary, which corresponds to the zero-crossing of γ^n in Fig. 3(a).

Summary. In conclusion, we have presented a formalism that provides full control over the electrical degrees of freedom in a periodic first-principles electronic-structure calculation. A novel and powerful aspect of the present approach is the ability to carry out calculations at fixed electric displacement field, which has important applications to the study of ferroelectric materials. Our procedure, developed and tested within a density-functional background, is very general and can be readily applied to any (quantum-mechanical or classical) theory of insulators in which the polarization can be rigorously defined. Using calculations on PbTiO_3 as a test case, we demonstrate that the method can be implemented efficiently and accurately, thus setting the stage for the theoretical study of polar instabilities in complex and large-scale ferroelectric systems, including technologically relevant heterostructures and capacitors.

Acknowledgements. This work was supported by the Department of Energy SciDac program on Quantum Sim-

ulations of Materials and Nanostructures, grant number DE-FC02-06ER25794 (M.S.), and by ONR grant N00014-05-1-0054 (D.V.).

-
- [1] R. D. King-Smith and D. Vanderbilt, Phys. Rev. B **47**, R1651 (1993).
 - [2] I. Souza, J. Íñiguez, and D. Vanderbilt, Phys. Rev. Lett. **89**, 117602 (2002).
 - [3] P. Umari and A. Pasquarello, Phys. Rev. Lett. **89**, 157602 (2002).
 - [4] O. Diéguez and D. Vanderbilt, Phys. Rev. Lett. **96**, 056401 (2006).
 - [5] D. Vanderbilt, Phys. Rev. B p. 7892 (1990).
 - [6] P. E. Blöchl, Phys. Rev. B **50**, 17953 (1994).
 - [7] D. Vanderbilt, J. Phys. Chem. Solids **61**, 147 (2000).
 - [8] X. Wu, D. Vanderbilt, and D. R. Hamann, Phys. Rev. B **72**, 035105 (2005).
 - [9] S. Baroni, S. de Gironcoli, and A. D. Corso, Rev. Mod. Phys. **73**, 515 (2001).
 - [10] J. P. Perdew and Y. Wang, Phys. Rev. B **45**, 13244 (1992).
 - [11] N. Troullier and J. L. Martins, Phys. Rev. B **43**, 1993 (1991).
 - [12] H. J. Monkhorst and J. D. Pack, Phys. Rev. B **13**, 5188 (1976).
 - [13] M. Stengel and N. A. Spaldin, Phys. Rev. B **75**, 205121 (2007).
 - [14] M. Stengel and N. A. Spaldin, Phys. Rev. B **73**, 075121 (2006).